Version 2.3 - 15 May 2000

Proposal for the RPC muon detector of LHCb

Università di Firenze and INFN, Firenze

Università degli Studi "Tor Vergata" and INFN, Roma

15 May 2000

Abstract

We propose to use RPCs to equip a substantial part of the muon detector stations M2–M5. RPCs made of phenolic plates of low resistivity ($\rho = 9 \cdot 10^9\ \Omega$ cm) and operated in avalanche mode offer very good performance and several advantages in region IV of M2–M5 and in region III of M4–M5. Using this technique it is possible to cover 75 % of the total area behind the calorimeters at moderate cost.

1 Introduction

The muon detector of experiment LHCb is made of 5 tracking stations, M1–M5. Resistive Plate Chambers (RPC) constitute a very attractive solution for equipping the outer region of stations M2–M5, located after the absorber, where the particle flux is relatively small [1]. RPCs are gaseous parallel-plate detectors that have several distinctive advantages, making them well suited for large-area fast trigger systems when spatial resolutions of order of centimeters are required [2]. In summary we quote:

- robustness and simplicity of construction (no wires)
- excellent timing properties:
  - unambiguous bunch-crossing identification (resolution better than 2 ns)
  - negligible dead-time effects (in avalanche mode)
- well adapted to inexpensive industrial production.

The readout of RPCs occurs via capacitive coupling to external strip or pad electrodes, which are fully independent of the sensitive element (the gas gap). This constitutes a further advantage of the detector.

The weak point of RPCs was the rate capability, but recently progresses have been made along this direction. Shifting the operation mode to avalanche rather than streamer (see later) allowed to reach rate capabilities of several kHz/ cm^2. In the LHCb muon detector the expected track density per cm^2 per interaction in stations M2 and M3 is shown in Fig. 1. In order to compute the particle flux, we multiply the curves by the interaction rate (10 MHz), and by a number of correction and safety coefficients yielding an overall factor of about 30 [3]. It is seen from the plots that detectors in region IV of station M2 (starting at about 2 m from the beam) will need to stand a flux ≤ 2 kHz/ cm^2. In stations M3–M5 the same limiting value is obtained around 1 m, corresponding to region III. RPC detectors built with low-resistivity phenolic plates can be used efficiently in these regions.

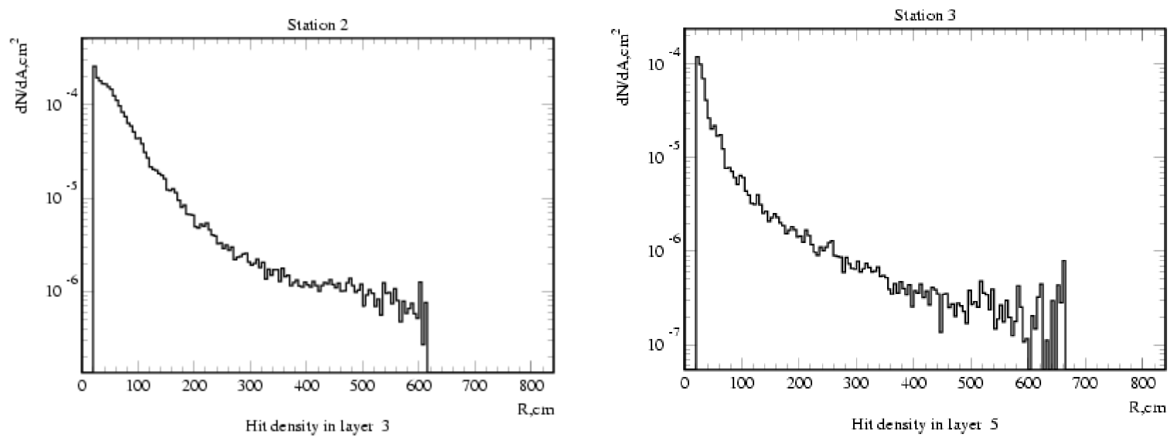

Figure 1 Charged track density/interaction in muon stations M2 and M3 (see text).

2 RPC detectors

2.1 Operating principles

2.1.1 Charge development

In Fig. 2 the working principle of the RPC is shown. Ionizing particles create electron-ion clusters in the gas, where an intense constant electric field is present between two parallel plates. An avalanche is created by multiplication in the gas, so that the cluster charge, q_0, becomes $Q = q_0 G(x) = q_0 \exp(\alpha x)$ after a distance x. α is the first Townsend coefficient and increases strongly with ratio of the electric field to the density. RPC operate at high gain, with $\langle G \rangle$ typically larger than 10^7. This is necessary since, in order to have high efficiency, the multiplication factor must be large even for those clusters that are created close to the positive electrode. Dense gases with high Z are preferred since have larger ionization probability.

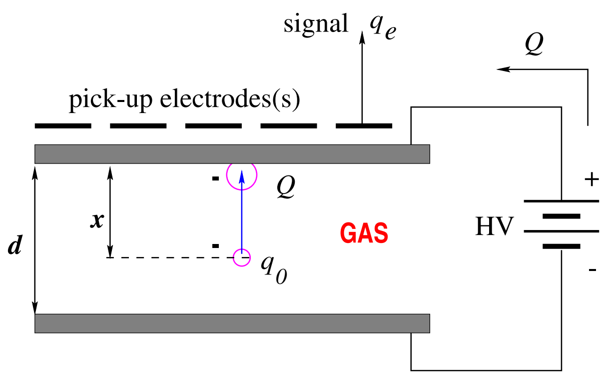

Figure 2 Principle of the RPC. Primary electron clusters, moving in the gas over a distance x, create an avalanche of final charge Q. A charge q_e is induced on the readout electrode(s).

2.1.2 Signal characteristics

The moving and growing avalanche induces images currents on the readout electrodes which can be computed theoretically by Green's theorem [4]. Given the characteristic exponential growth of the avalanche the output signal has a very fast risetime ($\tau \approx 1$ ns). Since the gain factor depends exponentially on x, a very large dynamic range results: typically the signal charge goes from 20 fC to 20 pC. A threshold of 20 fC is adequate to achieve full efficiency.

2.1.3 Streamer vs. avalanche mode

If the electric field is increased above a threshold which depends on the gas, the avalanche may be followed in time by a streamer. A rule of thumb says that this occurs when $\alpha d > 20$. The signal due to the streamers is much larger than the avalanche one, by at least one order of magnitude. In streamer mode the proportionality of the avalanche charge with the inducing charge is lost. When the electric field is further increased the avalanche-streamer delay decreases and the probability of generating streamers increases.

The presence of streamers was generally considered advantageous because the associated signal is large, however one must keep in mind that the avalanche (or the streamer) generated in the gas has the effect of discharging locally the electrodes. Thus a region around the trajectory of the ionizing particle becomes "blind" for a certain time until it is recharged. The area of electrodes discharged by the avalanche is proportional to the avalanche charge, and thus is much larger in streamer mode than in avalanche mode. Therefore operating the RPC in streamer mode must be avoided in order to work at high rates. It has been shown that efficient operation can be obtained also in avalanche mode, where the charge is limited to tens of pC [5]. Special gas mixtures, that reduce the creation of streamers, have also been developed.

2.1.4 Rate capability

Since the time constant for recharge is directly proportional to the bulk resistivity ρ of the electrodes (being of the order of milliseconds), the rate capability is proportional to $1/\rho$ and it is therefore desirable to have low-resistivity bakelite for the electrodes. Some RPCs with $\rho = 5 \cdot 10^8$ Ωcm have been succesfully tested, however there is no large experience in this region of resistivities. For industrial bakelite resistivities $\rho > 5 \cdot 10^9$ Ωcm are more common, and values of $10^{10} - 10^{11}$ are used by ATLAS and CMS [6] [7].

2.2 Specific requirements

Beyond the rate capability (2 kHz/ cm^2), time resolution and cluster size are important requirements. The cluster size (i.e. the number of adiacent strips fired simultaneously by a crossing particle) must be small in order to minimize the load on the trigger system. The requirements for the RPC detectors are summarized in Table 1.

In order to cope satisfactorily with high rate, the resistivity of the bakelite should be as small as practicable. We propose to use bakelite with resistivity of $9 \cdot 10^9$ Ω cm and thickness of 2 mm, which has been successfully tested by us and other groups up to > 3 kHz/ cm^2. Higher rates could be reached with lower resistivity, and we are in contact with the producers to perform tests of the new materials as soon as they become available.

Table 1 LHCb requirements for RPC.

Spatial efficiency per station	$> 99\%$
Rate capability (MIPs)	2 kHz/ cm^2
Rate capability (GIF test)	1 kHz/ cm^2
Time resolution	≤ 2 ns
Average cluster size	$\leq$?? strips (M3)
Max. radiation dose in 10 y	≤ 100 Gy

2.3 Types of detectors

We have considered two variants of the RPC detector, namely the single-gap RPC (SRPC) and the double-gap (DRPC). For both the basic building block is the gas gap, 2 mm thick and comprised between two phenolic sheets also 2 mm thick. These sheets are glued on a policarbonate frame (7 mm wide) and round policarbonate spacers (height 2.00 ± 0.01 mm) are glued in between, forming a rectangular grid of 100 mm pitch. The four gas inlets/outlets are placed close to the corners. A graphite layer is sprayed on the external surface of the bakelite planes in order to distribute the voltage. A PET insulating film (200 μm thick) is glued on the bakelite layer.

The frame gives a loss of about 2 % for a 2×1 m^2 RPC. The dead area associated with the spacers is 1 %.

In the SRPC there are usually two planes of readout strips (Fig. 3). These are placed close to the graphite (separated by the PET insulating layer)). The strips behave like transmission lines of 25-50 Ω impedance and must be terminated to avoid reflections and to minimize cross-talk. The polarity of the signal picked up being opposite for the two planes, the front-end electronics must be designed accordingly.

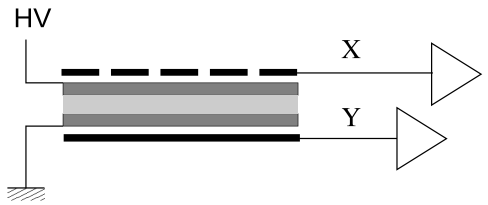

Figure 3 Layout of a singe-gap RPC with two readout planes.

The idea behind the DRPC is to increase efficiency by performing an analog OR of the signals from two gas gaps. In the DRPC different strip arrangements can be used (see Fig. 4) to achieve this. In the first case (a) the readout strip plane is sandwiched between two gas gaps [8] and therefore receives induction from both of them. In the second case (b) the strips are on the external side and are connected together. The OR connection can be at the level of the strips (before the preamplifier input) or after the preamplifier. In the latter case we have simply an OR of two SRPC.

CMS has chosen the layout (a). The price to pay is two gas gaps for a single coordinate, whereas two coordinates are possible with the single plane of the SRPC. The larger efficiency of the DRPC translates into a better rate capability and into an improved timing resolution.

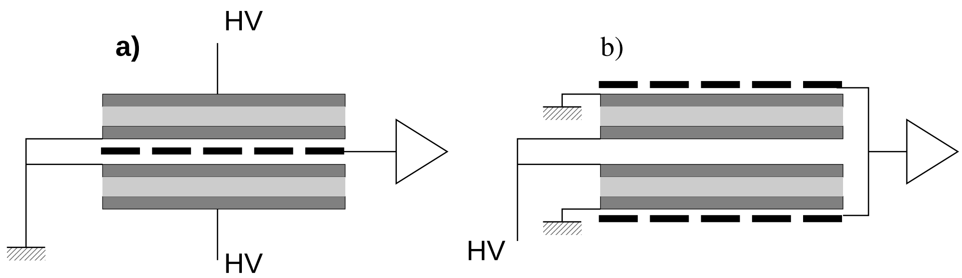

Figure 4 Layout of a double-gap RPC: a) with one readout plane, b) with two readout planes.

3 Detector performances

We have tested several type of detectors either on beam or at the CERN GIF facility, with particle fluxes up to 10 kHz/ cm^2 [9]. The detectors (dimensions 50×50 cm) were built with bakelite of $9 \cdot 10^9$ Ω cm resistivity.

The gas mixture consisted of 95 % $C_2H_2F_4$, 4 % isobutane and 1 % SF_6 [10]. $C_2H_2F_4$ is a non-flammable, environmentally safe gas. This gas is characterized by high density and large primary ionization ($>$ 60 primary ion pairs per cm). It has a relatively low operating voltage, low cost and easy availability. The percentage of isobutane is below the flammability threshold (5.75 %). SF_6 has the effect of reducing the formation of streamers.

For the readout electronics we used fast voltage amplifiers connected to the strips (widths of 2 and 3 cm), followed by discriminators and multi-hit TDCs. We used generally a threshold value of 60 mV, unless stated otherwise. Taking into account the preamplifier gain this corresponds to about 80 fC.

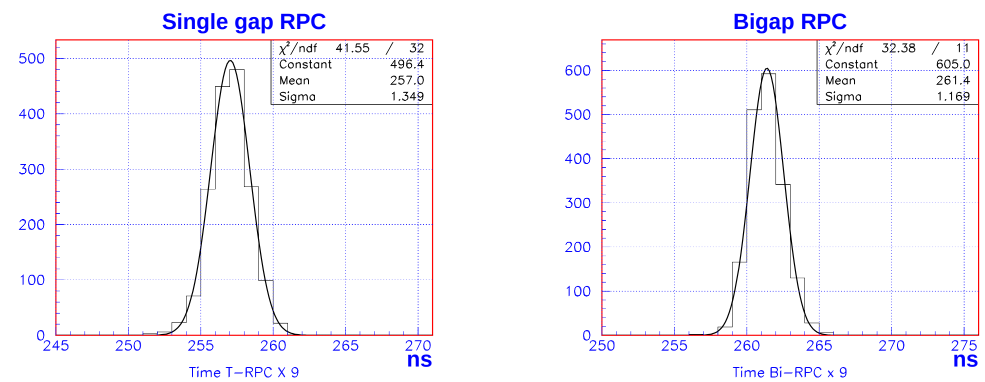

Figure 5 Time resolution for SRPC (left) and DRPC (right) (1 ns/ch)

3.1 Rate capability

3.1.1 T11 tests – . The data have been collected at the T11 pion beam at the CERN PS. The beam was approximately round in shape, with a FWHM of about 3 cm. We took data at several different intensities of the spill, corresponding to a flux between 0.5 kHz/ cm^2 and 10 kHz/ cm^2 in the central region of the beam spot.

Fig. 5 shows the time resolution for the SRPC and the DRPC. The timing resolution of the trigger scintillators has not been subtracted. The values obtained are $\sigma_t = 1.35$ ns for the SRPC and $\sigma_t = 1.17$ for the DRPC, with negligible tails.

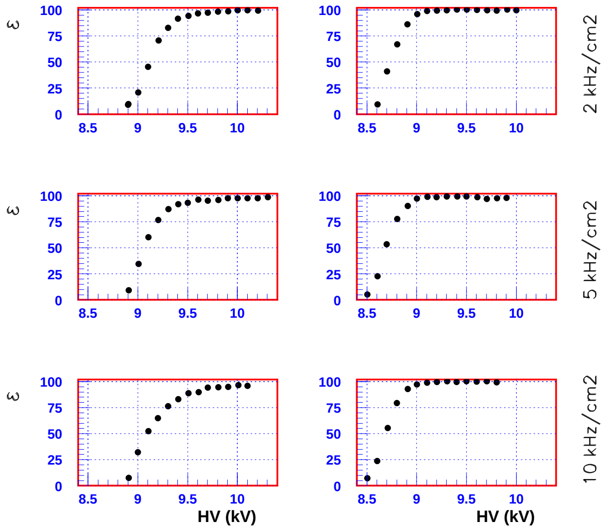

Figure 6 Efficiency curves for SRPC (left) and DRPC (right) at various beam intensities.

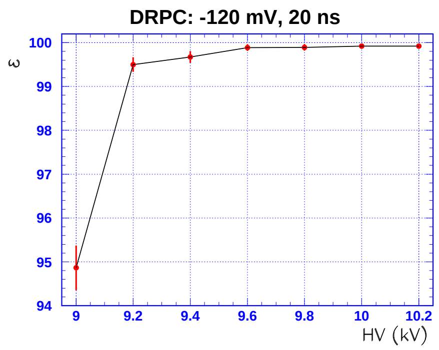

Figure 7 Efficiency curve for DRPC. Threshold 120 mV; gate: 20 ns; beam flux: 3 kHz/ cm^2

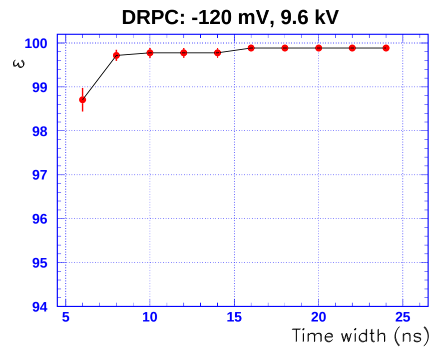

Figure 8 DRPC efficiency vs. gate width. Threshold 120 mV; HV = 9.6 kV; beam flux: 3 kHz/ cm^2

Fig. 6 shows the efficiency curves for the SRPC and DRPC under different beam intensity conditions. The DRPC shows clearly better efficiency at large rate, with almost no visible drop in performance up to 10 kHz/ cm^2. The SRPC shows some efficiency drop: at 9.8 kV ε decreases from 98 % at 2 kHz/ cm^2 to 96 % at 5 kHz/ cm^2. An expanded efficiency curve for the DRPC is shown in Fig. 7.

The excellent time resolution of the detector allows to get full efficiency already for gate widths of 8 ns (see Fig.8).

3.1.2 GIF tests – . The GIF (Gamma Irradiation Facility) at CERN is based on a very intense (740 GBq) ^{137}Cs source. The GIF is used to test detectors under continuous photon load, with fluxes comparable to those expected by the large LHC detectors. We could only test three SRPC detectors on the facility.

The GIF setup is shown in Fig. 9. The source is placed in a protected area on the X5 SPS beam line. A system of filters can be used to adjust the intensity of the 662-keV photons and to make it reasonably uniform over the area of the detectors. In this process the energy spectrum of the photons is considerably degraded. Because of this fact, the resulting flux is not strictly linear with 1/Attenuation [11]. At 1 m the counting rate achieved at minimum source attenuation (Att=1) corresponded to a flux of charged particles (photoelectric and Compton electrons) of 3.1 kHz/ cm^2. The sensitivity of the RPC to photons was derived to be $\varepsilon_\gamma \cong 1.2\ 10^{-3}$. The attenuation relevant for the LHCb working conditions is between 2 and 5 (see Table 1).

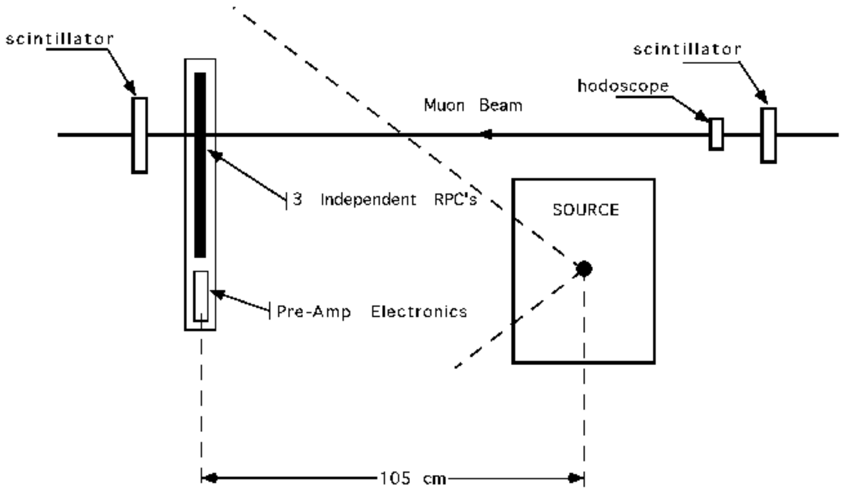

Figure 9 GIF test setup

The efficiency curves for muons as a function of the HV, with GIF Att = 50 and Att = 2 are shown in Fig. 10 and 11 for the X and Y readout of the three RPCs. At Att = 2 the onset of the plateau is displaced by about 300 V with respect to source off conditions. It has to be considered that, beyond the 1 % loss due to the spacers, at Att=2 the rate on the strips was as high as 400 kHz, introducing a dead time loss of about 1.5 %. The correction due to random was -0.5 %. In these conditions the three chambers still reach $>$ 95 % efficiency. At 10 kV and Att=1 the currents drawn by the chambers were about 0.2, 0.4 and 0.3 mA, corresponding to average cluster charges of 25-50 pC as expected for the avalanche mode of operation..

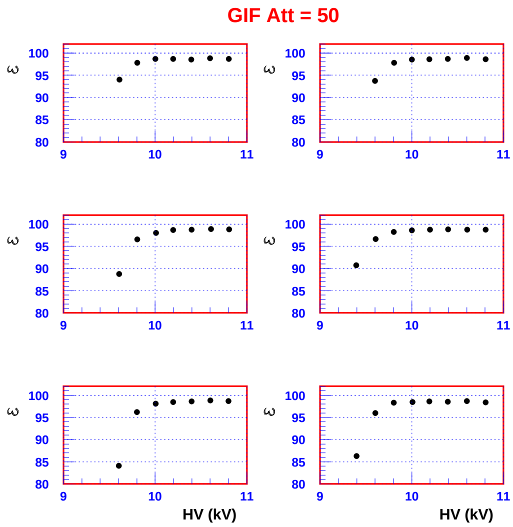

Figure 10 Efficiency curves for planes X (left) and Y (right) of the three SRPCs, for GIF attenuation 50 (flux 160 Hz/ cm^2).

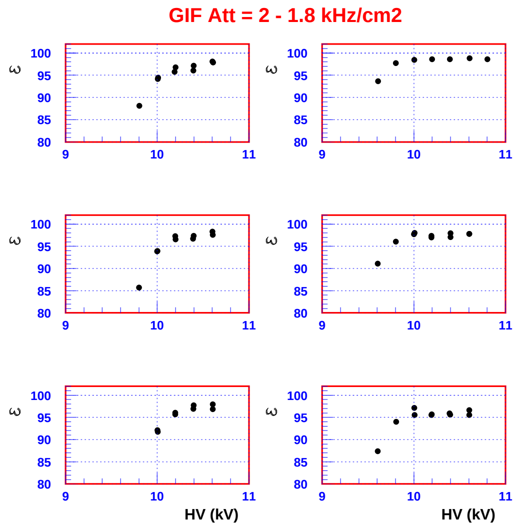

Figure 11 Efficiency curves for planes X (left) and Y (right) of the three SRPCs, for GIF attenuation 2 (flux 1.8 kHz/ cm^2).

3.2 Cluster size

Cluster size (i.e. the number of adiacent strips fired by a track) in LHCb is critical for the trigger performance and must be reduced as much as possible, in particular in station M3. In this respect LHCb is quite more demanding than ATLAS or CMS.

We have made a detailed experimental study of this parameter both for the SRPC and the DRPC. A quite good understanding of the underlying phenomena and a satisfactory agreement with calculations has been reached [12]. The cluster size h measured in RPCs has two origins: (i) a track passing close to the strip edge may induce a signal on the nearby strip large enough to be detected; (ii) cross-talk due to electromagnetic coupling between adiacent strips may result in large pulses firing three strips simultaneously.

Effect (i) is the same for both type of chambers (SRPC and DRPC), and is more important for narrow strips. Effect (ii) is related to the electrical structure of the readout strips and is larger in the DRPC because of the more "open" layout of the strip plane (the SRPC strips are close to a ground plane).

Fig. 12 (top) shows the average cluster size $\langle h \rangle$ and the efficiency (bottom) for an SRPC with 3 cm strips as a function of the beam position. The cluster size peaks to 2 in a region around the strip edges. It is about 1.2 in the middle of the strips. The edge effect (i) is important in a region $\approx \pm 7$ mm from the edges, in agreement with calculations. Effect (ii) is also in agreement with electrical measurements on the strip planes.

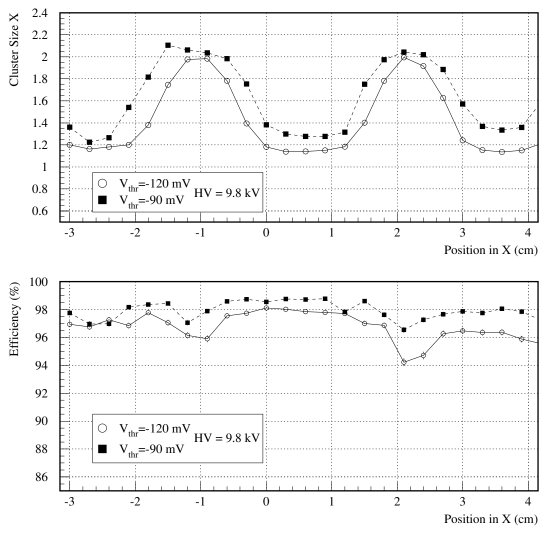

Figure 12 Average cluster size (top) and efficiency (bottom) versus beam position for an SRPC with 3 cm wide strips.

Fig. 13 shows the efficiency vs. $\langle h \rangle$ at different values of the threshold for a single SRPC (left) and for the OR of two SRPC (right). The plots show that a good efficiency plateau can be reached for values of $\langle h \rangle \approx 1.2 - 1.6$.

Fig. 14 shows separately the efficiency and the cluster size as a function of the HV (threshold 60 mV). The plateau is about 300 V.

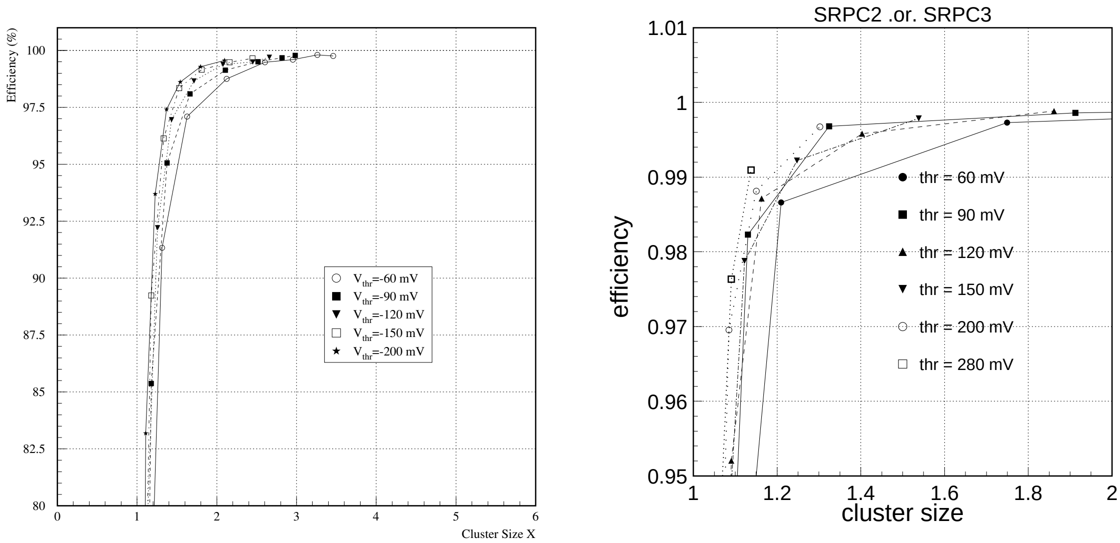

Figure 13 Efficiency vs. average cluster size for different values of the threshold. Left: single SRPC; Right: two SRPC in OR.

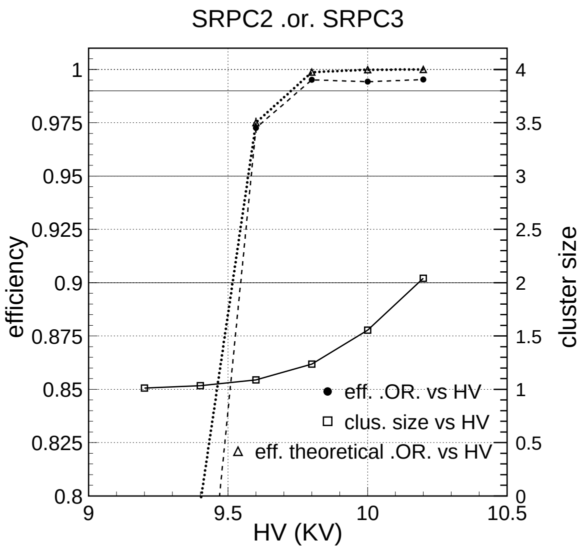

Figure 14 Two SRPC in OR. Efficiency and cluster size vs. HV. Threshold: -60 mV.

In the case of the DRPC the values are larger. At 99 % efficiency we obtained $\langle h \rangle \approx 3$. In this case the cross-talk contribution dominates and the value could probably be reduced (the CMS TDR quotes $\langle h \rangle < 2$) with a careful optimization of the electronics.

Finally it has to be stressed that all the results quoted here were obtained with strips of 50 cm length, whereas in the experiment the strips will be 50 % shorter, resulting in a corresponding decrease of the cross-talk. Therefore we are convinced that the RPCs will not cause any problem to the trigger.

3.3 Ageing properties

The mechanism of ageing in RPCs is totally different from that of wire chambers. In the RPC the the electric field is only marginally affected by deposits over a surface which is enormously larger than the tiny surface of the wires. A more serious concern could be due to changes in the characteristics of bakelite. In particular, increases of resistivity could affect the rate capability of the chambers.

RPCs have been in use for several years in L3 and no degradation of the performances has been detected, so dramatic changes of the electrical properties of bakelite due to “natural” ageing seem unlikely. Effects due to irradiation are probably more important in LHCb, where the maximum integrated dose in ten years for the RPC detectors is about 100 Gy [13].

To clarify if radiation can induce changes of the resistivity we have exposed different samples of bakelite to a gamma source, integrating a total dose of 20 kGy [1]. Values of ρ in the range $3\cdot 10^9 - 2\cdot 10^{12}\,\Omega$ cm were used. The results (see Fig. 15) show that the resistivity is not affected by radiation doses up to values 20 times higher than expected in LHCb.

These results agree with CMS, which has recently performed measurements on the GIF over a period of $7\cdot 10^6$ s, using an RPC with large resistivity ($4\cdot 10^{11}\Omega$ cm, so not well suited to large rates). The efficiency curves have been measured at different incident flux before and after exposition to the gamma source. With a total absorbed dose of 20 Gy, there was a negligible effect at 1.3 kHz/ cm^2 (Att=5) [14].

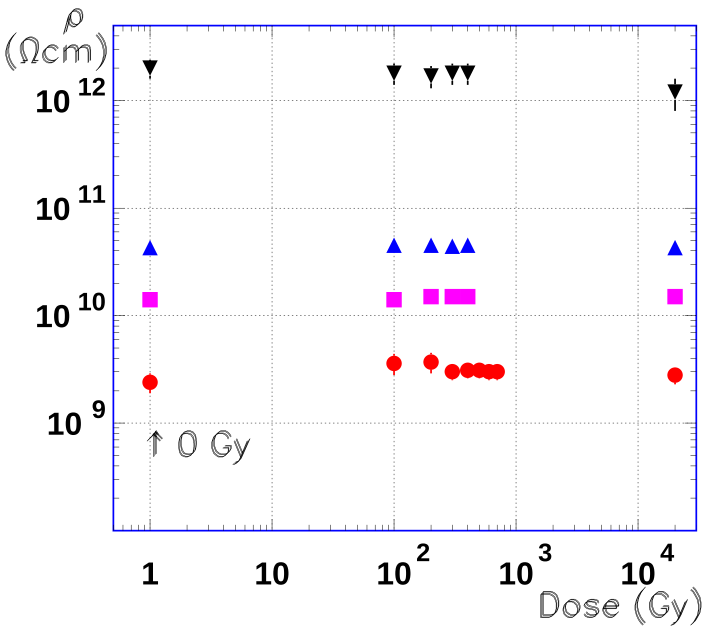

Figure 15 Resistivity of different bakelite sample before and after irradiation with ^{60}Co gammas. 100 Gy = integrated dose for 10 years in LHCb.

[1]We are grateful to C. Bosio for helping us with this measurements.

4 RPC construction

There is today a wide experience in industrial production of RPCs. The procedure for construction and the necessary tooling was developed several years ago by R. Santonico in collaboration with industry, and was succesfully used in L3 and BABAR. This procedure has been continuously refined by R&D work for ATLAS and CMS, so we are confident that the production of the RPCs gaps can be made in industry. The production process has however to be closely monitored to ensure the quality of the chambers. In particular, the selection of the bakelite (resistivity and surface roughness) will be under the direct responsibility of the institutes. For the details of manifacturing, please refer to the ATLAS and CMS TDRs [6],[7].

The production capability in the industry is about 15 single-gaps/day. This is adequate for us, since the total number of single-gaps needed is about 1700 (see below).

5 Station layout

5.1 Redundancy considerations

A very important requirement of the muon system is to have a high protection against possible chamber malfunctions. To ensure adequate redundancy the double-gap solution is the most appropriate. The two gaps will be powered independently: in this way one of the gaps could be shut down in case of problems, with a modest loss in efficiency only in the high-rate regions [2]. The simplest way to combine two gas gaps is the DRPC, where only one readout plane is shared between the gaps (Fig. 4 a). However a slightly different approach, with two SRPC combined in OR could prove to be better (Fig. 4 b)). The optimum solution will be chosen having in mind specially the minimization of the cluster size. Solutions like the majority of 3 SRPC planes have been considered and tested with good results, but they are more complicated and expensive, and the advantage in terms of random noise suppression does not seem to be enough to justify them.

5.2 Efficiency considerations

The demanding requirements on spatial efficiency (see Table 1) led us to discard separate readout strips for the X and Y coordinates. We will use a geometry very much similar to the WPC's one, having short strips oriented vertically. The short strips will be grouped horizontally to form physical "pads", which will be then OR-ed horizontally and vertically to form the logical strips going to the trigger. The maximum length of the strips will be 30 cm in M5. The short length will also help in reducing cross-talk effects thus improving the cluster size.

5.3 Chamber dimensions

The layout in the four stations M2 – M5 is based on chambers with two separate layers of SRPC, thus requiring 2 gas gaps. The alternative uses only one layer of DRPC in each chamber and allows a more compact arrangement and a 50 % saving in front-end channels. The

[2] This does not necessarily require doubling of number of HV channels. ATLAS envisages to use special HV distributors which allow to switch on/off independently several RPCs on the same HV supply.

total thickness available between the iron plates is 360 mm, which is more than adequate to accomodate the necessary overlaps.

The chambers for region III and IV will have the same width inside a station (from 1.2 m in M2 to 1.5 m in M5). The strips will be 0.25 – 0.3 m long (L) in region IV, and half this size ($L/2$) in region III. Some extra length will be added to allow for the vertical overlap the readout planes.

In order to minimize the problems of overlap and dead space at the boundary between regions III and IV, the simplest solution is to have chambers of the same height L everywhere. Chambers in region III will have the strips of length $L/2$ read from the upper or the lower side and with negligible dead space in between [3].

The propagation delay of 5.5 ns/m yields for the longest strips a time spread of 0.45 ns, i.e. totally negligible.

Table 2 gives the detailed list of dimensions and the number of the chambers. The number of gas gaps is twice the number of chambers, giving a total of 1728. This choice results in a fairly large number of gas gaps to build. From the general point of view of view, there would be a clear advantage in using larger gas gaps, since larger chambers are more economical to build (faster assembly, less HV and gas connectors) and the extension of boundaries is minimized. It would be entirely possible to build larger gas gaps (e.g. around 1 m vertically) without changing the segmentation of the readout strips, therefore we will investigate thoroughly this possibility keeping in mind in particular the constraints imposed by the integration with the Wire Chambers.

Table 2 Chamber sizes for the RPC stations. A single "chamber" is made of 2 gas gaps (see text) and in region III the strips are read out on the upper and on the lower side. Number of gas gaps: $2 \times 864 = 1728$.

Station	Region	No. chambers	X dim (mm)	Y dim (mm)	Area (m^2)
M2	IV	192	1200	250	58
M3	IV	192	1300	270	68
M4	III	48	1400	290	20
M4	IV	192	1400	290	78
M5	III	48	1500	310	22
M5	IV	192	1500	310	89
Total		864			335

5.4 Dead spaces

In order to minimize dead space effects at the boundary between two readout planes, a possible solution can be seen in Fig. 16. The gas gaps are staggered along the horizontal direction, in such a way that the readout strip layer always sees at least one gas gap. In this way the transition zone will have a slightly reduced efficiency (better in any case than 95 %, see Sect. 3.1.2) and the total loss is a second-order effect.

[3] It is possible to insert the terminating resistors on the two head-to-head strips without taking any extra space. Due to the shortness of the strips, however, it is probable that no termination will be needed.

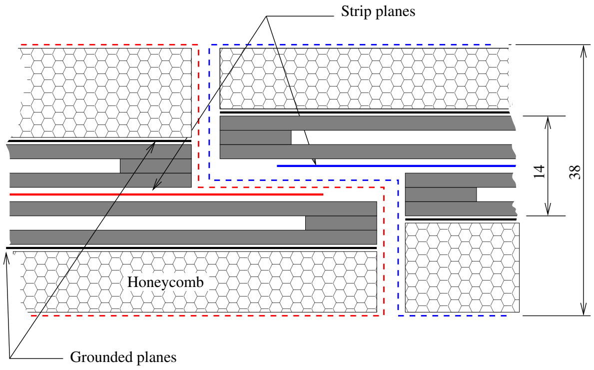

Figure 16 Possible layout in the overlapping region of DRPC readout planes.

The assembly is kept in place by means of honeycomb support panels that ensure the necessary rigidity to all the chamber structure. The completed chamber has a thickness of about 40 mm. Along the orthogonal (the vertical) direction the dead space is avoided by overlapping the chambers like in Fig. 17.

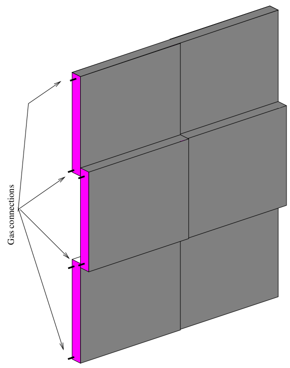

Figure 17 Overlapping of the chambers.

5.5 Readout strips

The width of the readout strips must be an integer fraction of the logical strip width. We have chosen the fraction in such a way to have strip sizes not much different from 3 cm, thus mantaining the same impedance everywhere (about 30 Ω). With this choice every chamber in region III has 192 strips (96 per gap) and 96 strips (48 per gap) in region IV.

The number of physical strips participating in a logical strip varies between 2 (in M2) and 10 (in M5).

Table 3 gives the strip widths and the total number of channels for DRPC with independent readout of both gaps (layout b) of Fig. 4)

The number of channels could be reduced considerably in three ways:

i). using the DRPC layout a), since the readout plane is shared by the two gaps;

ii). using layout b) and OR-ing the strips before the preamplifiers;

iii). using wider strips.

Table 3 Tentative strip sizes and physical channel count for the RPC stations. We assume two independent strip planes for each chamber (i.e. one per gas gap, see text).

Station	Region	No. chambers	X strip (cm)	Strips/ch.	Total channels
M2	IV	192	2.5	96	18432
M3	IV	192	2.7	96	18432
M4	III	48	2.9	192	9216
M4	IV	192	2.9	96	18432
M5	III	48	3.1	192	9216
M5	IV	192	3.1	96	18432
Total		864			92160

Solution *i*) can be used if the cluster size of the DRPC can be made small enough, and most likely could be employed already in stations M4 and M5 where a logical strip is made of several physical strips.

Solutions *ii*) and *iii*) have to be verified experimentally because of the increased strip capacitance. In Tor Vergata tests are under way for the pad readout of RPC (TOTEM experiment) and their results will be very useful for us. Therefore the values of Table 3 should be taken as upper limits. Concerning the problems of dead time introduced by the front-end electronics, the present solution gives a maximum rate of 2 kHz/ $\mathrm{cm}^2 \times 62.5\ \mathrm{cm}^2 = 130$ kHz. Even using the relatively slow CMS chip (see below) the maximum loss is below 1 %.

5.6 Chamber production

The assembly of the RPC gas gaps and of the strips to form a complete chamber will be made in the industry. These chambers will then be delivered to the institute laboratories, where the front-end electronics will be mounted. Finally several chambers in parallel will be tested with cosmic rays. From six to twelve months should be necessary to perform this task. The chambers will then be shipped to CERN.

5.7 Station assembly

This will be made at CERN.

6 RPC front-end electronics

Two possibilities exist: (1) the ATLAS chip and (2) the CMS chip. Both chips have 8 channels comprising integrated amplifier-shaper-discriminator and have been designed specially for RPCs. Circuit (1) is built in GaAs and is only available in die form, thus requiring to be bonded to the circuit board. It is a voltage amplifier followed by a discriminator and output

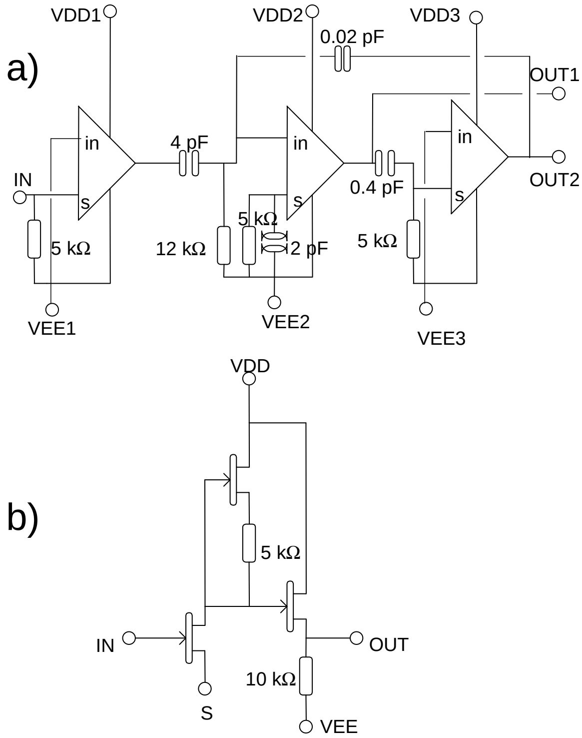

Figure 18 Block diagram of the ATLAS front-end GaAs chip: a) interconnection of the three stages; b) sketch of the single stage.

circuit (Fig. 18), and requires a step-up transformer as a part of the multilayer front-end board to adapt the strip impedance to the input. The necessity of bonding and of the step-up transformer are complications whose associated extra costs need to be carefully evaluated, even if the chip itself has a very attractive price.

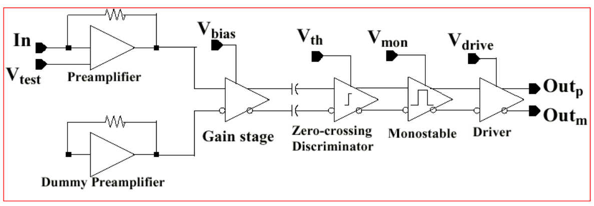

Figure 19 Block diagram of the CMS front-end BiCMOS chip.

Circuit (2), built in BiCMOS technology, is shown schematically in Fig. 19. The transimpedance preamplifier is adapted to the strip line and is followed by a zero-crossing discriminator and LVDS driver. It comes in a PQFP 80 64-pin plastic case [15].

Concerning the rate capability, circuit (1) is be capable of operation up to 100 MHz, whereas circuit (2) has a monostable in the output circuit which introduces a dead time of 50 ns.

We plan to test both circuits and to carefully compare their performances in connection with our DRPC detectors. In particular (i) the time resolution, (ii) the dead-time requirements and (ii) the cluster width will be considered in the comparison.

7 HV system

8 Gas system

9 Cost estimate

9.1 Construction costs

The cost for the construction of a complete chamber is summarized in Table 4 in CHF/ m^2. The total area to be covered is 335 m^2, thus giving a total cost is about 250 kCHF. For DRPC the main difference is only one strip plane, giving a cost reduction of 35 CHF.

Table 4 Detail of costs for production of chambers made of two SRPC in OR.

Item	Cost per m^2
Bakelite	80 CHF
Assembly	300 CHF
Strip planes (2)	80 CHF
HV Connectors (2 pairs)	50 CHF
Extras	140 CHF
Total	650 CHF

9.2 Electronics costs

The cost is dominated by the front-end electronics: at a price of 6 CHF/channel (including the chip, the boards and the cables) we have about 550 kCHF, that must be considered as an upper limit.

References

[1] LHCb Technical Proposal, CERN/LHCC 98-4, 1998.

[2] R. Santonico and R. Cardarelli, Nucl. Instr. and Meth. in Phys. Res. 187 (1981) 377.

[3] R. LeGac, A. Tsaregorodtsev, V. Talanov, LHCb Note 99-036 (1999).

[4] See e.g. V. Radeka, Ann. Rev. Nucl. Part. Sci. 38, (1988) 217;
E. Gatti, G. Padovini, V. Radeka, Nucl. Instr. and Meth. in Phys. Res. 193 (1982) 651.

[5] R. Cardarelli, A. Di Ciaccio and R. Santonico, Nucl. Instr. and Meth. in Phys. Res. A 333 (1993) 399;
C. Bacci et al., Nucl. Instr. and Meth. in Phys. Res. A352 (1995) 552;
R. Cardarelli, V. Makeev, R. Santonico, Nucl. Instr. and Meth. in Phys. Res. A 382 (1996) 470.

[6] ATLAS muon TDR, CERN/LHCC/97-22, (1997).

[7] CMS muon TDR, CERN/LHCC/97-32, (1997).

[8] T. Moers et al., Nucl. Instr. and Meth. in Phys. Res. A 345 (1994) 474.

[9] M. Adinolfi et al., LHCb Note 99-049 (1999).

[10] P. Camarri et al. Nucl. Instr. and Meth. in Phys. Res. A 414 (1998) 317.

[11] When scaled for the different distances, our results agree with those reported by M. Maggi et al, Proc. IV Int. Workshop on RPC and Related Detectors, Scientifica Acta Univ. Pavia, vol XIII n.2 (1998) 139.

[12] For a simple model see G. Carboni and G. Passaleva, LHCb Note (in preparation).

[13] V. Talanov, LHCb Note 97-017 (1997) and private communication.

[14] G. Pugliese, talk given at the 5th Int. Conf on Position-Sensitive Detectors, London (1999).

[15] F. Loddo, talk given at the V Int. Workshop on RPC and Related Detectors, Bari (1999).